Journal of Chromatography A, 1218 (2011) 32–45

Contents lists available at ScienceDirect

Journal of Chromatography A

journal homepage: www.elsevier.com/locate/chroma

Effective medium theory expressions for the effective diffusion in chromatographic beds filled with porous, non-porous and porous-shell particles and cylinders. Part I: Theory

Gert Desmet*, Sander Deridder

Vrije Universiteit Brussel, Department of Chemical Engineering, Pleinlaan 2, 1050 Brussels, Belgium

ARTICLE INFO

Article history:
Received 8 July 2010
Received in revised form 5 October 2010
Accepted 25 October 2010
Available online 30 October 2010

Keywords:
B-term
Longitudinal diffusion
Peak parking
Effective Medium Theory
Modelling
Permeability

ABSTRACT

Using the permeability analogue of the diffusion and partitioning processes occurring in a chromatographic column, the different Effective Medium Theory (EMT) models that exist in literature for the electrical and thermal conductivity have been transformed into expressions that accurately predict the *B*-term band broadening in chromatographic columns. The expressions are written in such a form that they hold for both fully porous and porous-shell particles, and both spherical and cylindrical particles are considered. Mutually comparing the established EMT-expressions, it has been found that the most basic variant, i.e., the Maxwell-based expression, is already accurate to within 5% for the typical conditions encountered in liquid phase chromatography, independently of the exact microscopic morphology of the packing. For most typical values of the intra-particle diffusion rate and the species retention factors, it is even accurate to within 1%. If even higher accuracies are needed, more elaborate EMT-expressions are available. The modelling accuracy of all explicit EMT-expressions is much better than the residence time weighted (RTW) *B*-term expressions that have been used up to now in the field of chromatography, where the error is typically on the order of 10% and more. The EMT-models have also been used to establish expressions for the obstruction and tortuosity factor in packings of non-porous particles. The EMT has also been applied to the meso-porous zone only, yielding an expression for the intra-particle diffusion coefficient that can be used without having to specify any obstruction factor. It has also been shown that the EMT also provides a very simple but exact expression to represent the way in which the solid core obstructs the effective intra-particle diffusion in the case of porous-shell particles. This obstruction factor is given by $\gamma_{part} = 2/(2+\rho^3)$ for spherical particles and $\gamma_{part} = 1/(1+\rho^3)$ for cylinders. Back-transforming the obtained expressions, a set of simple explicit expressions has been obtained that allow to directly obtain the intra-particle diffusion coefficient (D_{part}) from peak parking or *B*-term constant measurements. Using these expressions, it could be demonstrated that the traditionally employed RTW-model yields D_{part}-values that display an erroneous retention factor dependency, even in cases where the RTW-model appears to be able to closely fit the peak parking measurements.

1. Introduction

In the field of chromatography, the contribution of the longitudinal diffusion (usually referred to as *B*-term band broadening) to the total band broadening is traditionally written as [1]:

$$H_B = \frac{2D_{eff}}{u_0}(1+k') \quad (1)$$

Switching to dimensionless variables, and putting:

$$\gamma_{eff} = \frac{D_{eff}}{D_m} \quad (2)$$

Eq. (1) becomes:

$$h_B = \frac{B}{\nu_0} = \frac{2\gamma_{eff}}{\nu_0}(1+k') \quad (3)$$

with

$$B = 2\gamma_{eff}(1+k') \quad (4)$$

Thus far, the effective longitudinal diffusion has nearly always been described using the parallel-zone or residence time weighted (RTW) model introduced by Knox [1], Stout and De Stefano [2] and Giddings [3]. In 2008, our group [4,5] however showed that the

* Corresponding author. Tel.: +32 02 629 32 51; fax: +32 02 629 32 48.
E-mail address: gedesmet@vub.ac.be (G. Desmet).

0021-9673/$ – see front matter © 2010 Elsevier B.V. All rights reserved.
doi:10.1016/j.chroma.2010.10.087

conventionally used residence time weighted model (RTW-model) is intrinsically incorrect and can even violate the fundamental diffusion limits. It was also pointed out that it should be possible to obtain much more accurate representations of the effective longitudinal diffusion using the Effective Medium Theory (EMT), as is done in many other fields of science and technology where the EMT is fully accepted as a powerful approach to, for example, calculate effective optical transmission coefficients, elasticity moduli, and heat transfer and diffusion coefficients of binary media [4,6,7]. One of the EMT-expressions, i.e., the one established by Maxwell, is widely accepted in the field of chemical engineering to represent the diffusion in packed bed columns [8]. In the field of chromatography, the EMT has already been used to measure the effective tortuosity in suspensions and packings of porous particles, as well as inside the particles [9]. In [4,5], the EMT has been used to model the effective diffusion under chromatographic conditions (comprising both diffusion and preferential phase distribution) in periodic arrays of cylinders and to study the stationary phase diffusion coefficient in porous particles. Very recently, the possibility to use the EMT to predict the longitudinal diffusion has also been recognized by Gritti et al. [10,11]. They however indicate that the difference between RTW-model and the EMT-model they used, is too small to reject either of them.

The present study aims at resolving this debate. First, it needs to be considered that a variety of EMT-models exist, with a varying degree of accuracy. Globally, the EMT-models can be divided in three subdivisions: explicit models (Maxwell-type approximations), self-consistent models (Bruggeman- and Landauer-models) and differential medium approximation models [6]. The paper that initiated the explicit EMT-modelling work is undoubtedly that of Maxwell [12], already dating back from 1873. His work has later been extended by, amongst others, McPhedran and McKenzie [13], Sangani and Acrivos [14], Torquato [15] and Cheng and Torquato [16]. Through the course of history, these authors have established the explicit models for the effective conductivity in periodic arrays or random packings of conducting spheres in a mathematically rigorous way. Whereas the original Maxwell-expression is only exact for dilute suspensions of spheres, the more advanced expressions established by his successors also take near-neighbour interactions into account.

Most EMT-expressions have originally been established to calculate the effective thermal and electrical conduction of a binary medium. For reasons of mathematical analogy, the EMT-expressions also hold for properties such as the dielectric constant, the magnetic permeability and the diffusion coefficient [6]. None of these processes however involve the occurrence of a partitioning or preferential solubility effect between the two phases, whereas this is clearly the case when considering the diffusive process in a chromatographic column. As such the latter problem bears a perfect similarity with the permeation of analytes through composite media and membranes [17]. Recognizing that the correct driving force for the diffusion in the presence of a preferential solubility is the gradient in chemical potential and not the gradient in concentration, Davis [7] has shown that the correct property that obeys the EMT-rules is the permeability and not the diffusivity. Up to now, only the Maxwell- and the Landauer–Davis model have been formulated in terms of the effective permeability problem [4,18], but most of the EMT-models that have a higher order accuracy have not been adapted yet.

In what follows, we have therefore transformed all relevant explicit and implicit EMT-expressions for the effective conductivity in binary media that can be found in literature into expressions for the D_{eff}-factor and the B-term constant in chromatographic columns. We also considered the expression derived by Hashin and Shtrikman [19] who extended the realm of EMT-expressions to coated-spheres systems (i.e., to ternary media consisting of a packing or suspension of spheres with a core and a concentric shell with a different conductivity). Obviously, their solution directly opens the road to the treatment of the case of porous-shell particles.

The EMT-expressions for the conductivity in 2D ordered and disordered cylinder packings are considered as well, because they allow to predict the B-term constant in so-called COMOSS or micropillar array columns (μPAC's) [20–22]. To some approximation, cylinders can also be used to represent the skeleton of monolithic columns [23]. In part II of the present study, the expressions obtained in this part are validated by comparing them against a set of highly accurate numerical calculations.

Subsequently, the different obtained B-term constant expressions have been mutually compared for their general accuracy and their sensitivity to the exact geometry of the packing (Section 3). In addition, we also established the inverse expressions, allowing to accurately extract the value of the intra-particle diffusion coefficient from a measured value of the effective longitudinal diffusion coefficient (Section 5).

2. Formulation of the EMT-expressions in terms of the macroscopic chromatographic parameters

To apply the EMT to the problem of diffusion in a chromatographic column, the column first needs to be represented as a binary medium consisting of two zones, zone$_1$ (=interstitial void, volumetric fraction ε_e) and zone$_2$ (=particles, volumetric fraction $1-\varepsilon_e$), each with uniform but distinct physicochemical properties (Fig. 1a).

To subsequently transform the literature EMT-expressions into expressions for the effective permeability problem, and from thereon to expressions for the effective diffusivity, the approach adopted in [4] can again be used. In this approach, one distinguishes between the permeability P_{part} of the particle zone and the permeability P_{m} of the mobile zone (i.e., the interstitial void zone), each defined as the product of the solubility S and the diffusion coefficient D experienced by the analytes in the given zone:

$$P_{\mathrm{m}} = D_{\mathrm{m}} S_{\mathrm{m}} \quad \text{and} \quad P_{\mathrm{part}} = D_{\mathrm{part}} S_{\mathrm{part}} \tag{5}$$

It should be noticed that the concept "solubility" [18] is used here as a synonym for a partition coefficient describing the equilibrium partition with respect to a neutral medium with solubility $S = 1$.

Subsequently exchanging conductivities with permeabilities in the EMT-expressions for the effective conductivity then directly provide an expression for P_{eff}, the effective permeability of the binary medium. In analogy with Eq. (5), this P_{eff} can also be expressed as the product of the effective diffusion coefficient D_{eff} and the effective solubility S_{eff} [7,17]:

$$P_{\mathrm{eff}} = D_{\mathrm{eff}} S_{\mathrm{eff}} \tag{6}$$

with the effective solubility S_{eff} being defined as:

$$S_{\mathrm{eff}} = \phi_{\mathrm{m}} S_{\mathrm{m}} + \phi_{\mathrm{part}} S_{\mathrm{part}} \tag{7}$$

Taking the solubility in the mobile phase as unity ($S_{\mathrm{m}} = 1$), the particle-based solubility S_{part} appearing in Eqs. (5) and (7) is simply equal to the whole-particle based equilibrium distribution constant K_{part} defined in the Supplementary material (SM):

$$K_{\mathrm{part}} = \frac{S_{\mathrm{part}}}{S_{\mathrm{m}}} = \frac{m_{\mathrm{part,eq}}/V_{\mathrm{part}}}{C_{\mathrm{m,eq}}} \tag{8}$$

This equilibrium constant expresses the relation between the total mass (or moles) of species present in the particle in equilibrium with that present in the interstitial void volume.

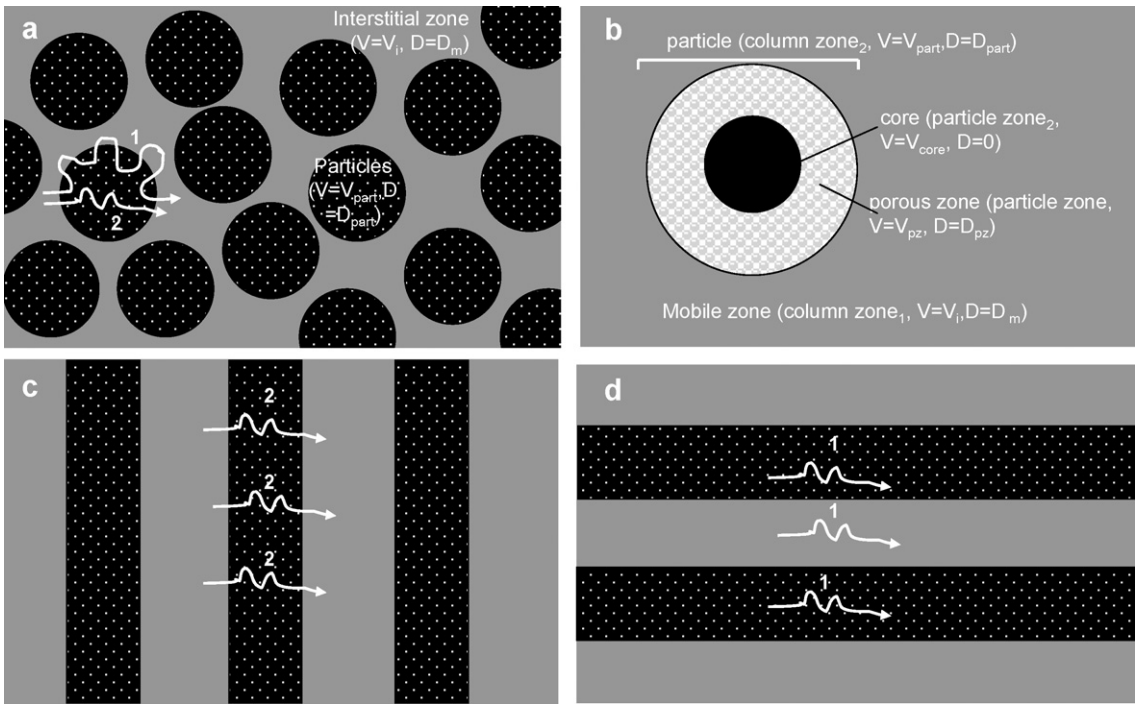

Fig. 1. (a) Schematic representation of a packed bed column consisting of porous particles (dark regions) embedded in the mobile phase liquid filling up the interstitial void (light continuous region). Trajectory (1) and (2) respectively represent a purely parallel- and purely serially-connected diffusion path. (b) Zoom-in of a porous-shell particle. (c, d) System wherein same amount of meso-porous material as in (a) is distributed in (c) a purely serial orientation and (d) a purely parallel orientation.

With the above definitions and conventions, the ϕ- and S-parameters appearing in Eqs. (5)–(8) can be written as:

$$\begin{cases} \phi_1 = \varepsilon_e \\ \phi_{part} = 1 - \varepsilon_e \\ S_1 = 1 \\ S_{part} = K_{part} \end{cases} \tag{9}$$

As shown in the SM, K_{part} can be directly linked to either the zone retention factor k'' (k_1 in [10] or δ_1 in [24]) or to the phase retention factor k' by the generally valid expression:

$$K_{part} = \frac{\varepsilon_e}{1-\varepsilon_e} k'' = \frac{\varepsilon_T}{1-\varepsilon_e}(1+k') - \frac{\varepsilon_e}{1-\varepsilon_e} \tag{10}$$

As defined by Knox [25], the zone retention factor k'' relates the analyte retention time to the residence time of a marker that only occupies the interstitial void and does not enter the particles, whereas the phase retention factor k' relates the analyte retention time to the residence time of the unretained marker (t_0-time). Both quantities are related via Eqs. (S-4) or (S-13) of the SM.

Before proceeding, it is also convenient to introduce α_{part} as the ratio of the permeability of the particle zone over that of the interstitial zone, further referred to as the "relative particle permeability":

$$\alpha_{part} \equiv \frac{P_{part}}{P_m} = \frac{K_{part} D_{part}}{D_m} \tag{11}$$

Using Eqs. (10) and (11), α_{part} can also be conveniently rewritten as a function of k' and k'':

$$\alpha_{part} = \frac{\varepsilon_e k''}{1-\varepsilon_e} \cdot \frac{D_{part}}{D_m} = \frac{(1+k')\varepsilon_T - \varepsilon_e}{1-\varepsilon_e} \cdot \frac{D_{part}}{D_m} \tag{12}$$

This α_{part} is the equivalent of the thermal or electrical conductivity appearing in the traditional literature EMT-expressions, and can hence readily replace the latter when treating an effective permeability problem.

2.1. Explicit models (spherical particles)

Traditionally, the explicit EMT-expressions are simplified by introducing the parameter β_1, usually referred to as the polarizability constant [15], and depending exclusively on α_{part}:

$$\beta_1 = \frac{\alpha_{part} - 1}{\alpha_{part} + 2} \tag{13}$$

2.1.1. Maxwell-based expression

Using Eq. (13), and taking the conductivity of the medium surrounding the particles as σ_m, the basic Maxwell-expression for the effective thermal or electrical conductivity of a suspension of particles embedded in a uniform medium is typically written as [15,26]:

$$\frac{\sigma_{eff}}{\sigma_m} = \frac{1 + 2\beta_1(1-\varepsilon_e)}{1 - \beta_1(1-\varepsilon_e)} \tag{14}$$

Replacing now the thermal or electrical conductivity σ by the permeability P, and using the relation between P_{eff} and D_{eff} given by Eq. (6), it is found that:

$$\frac{D_{eff}}{D_m} = \frac{1}{S_{eff}} \cdot \frac{P_{eff}}{D_m} = \frac{1}{S_{eff}} \cdot \frac{1 + 2\beta_1(1-\varepsilon_e)}{1 - \beta_1(1-\varepsilon_e)}, \tag{15}$$

which, upon using the expressions for B, γ_{eff} and S_{eff} given in Eqs. (2), (4) and in Eq. (S-20) of the SM, can be written as:

$$B = 2\gamma_{eff}(1+k') = \frac{2}{\varepsilon_T} \cdot \frac{1 + 2\beta_1(1-\varepsilon_e)}{1 - \beta_1(1-\varepsilon_e)} \tag{16}$$

2.1.2. Rayleigh-based expression

One of the assumptions underlying the Maxwell-model is that of a dilute suspension, wherein the conductivity in a given particle is not influenced by the conductivity in the neighbouring particles. To take these close-neighbour interactions into account, some additional information about the local packing geometry needs to be included in the calculations. This was first done by Rayleigh [27], who considered the case of a face centered cubic (fcc) packings of spheres (see Fig. 2a) and succeeded in finding the higher

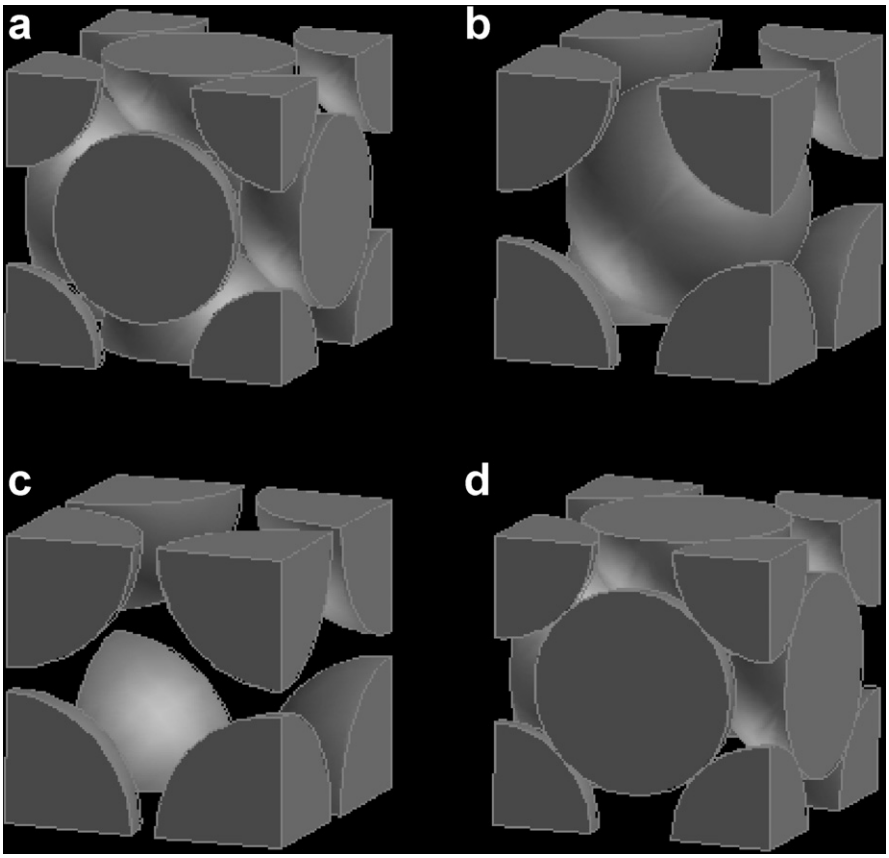

Fig. 2. Unit cells of (a) a face centered cubic (fcc), (b) a body centered cubic (bcc) and (c) a simple cubic (sc) sphere packing. (d) Unit cell of an fcc-packing at the close-packing limit.

order terms needed in the non-dilute suspension or packing case. Using the same transformations as those used to obtain Eq. (16), his solution can be written as:

$$B = 2\gamma_{\text{eff}}(1+k') = \frac{2}{\varepsilon_T}\left(1-3(1-\varepsilon_e)[-\frac{1}{\beta_1}+(1-\varepsilon_e)-1.569\cdot\frac{1-\alpha_{\text{part}}}{4+3\alpha_{\text{part}}}\cdot(1-\varepsilon_e)^{10/3}+\cdots]^{-1}\right) \quad (17)$$

2.1.3. Highest order accuracy solutions

Eq. (17) contains only one higher order term and there has been serious doubt about its possibility to converge to the exact solution [14]. It was not until the availability of a sufficient computational power and the work of McPhedran and McKenzie [13], Sangani and Acrivos [14], and finally Cheng and Torquato [16,26] that highly accurate explicit expression for the three existing types of ordered sphere packings (see Fig. 2: simple cubic (sc), body centered cubic (bcc) and face centered cubic (fcc) packing) were obtained. The expression established by Cheng and Torquato [16] for example has a 9th order accuracy in the particle fraction [26], and can be written as:

$$B = 2\gamma_{\text{eff}}(1+k') = \frac{2}{\varepsilon_T}\left(1-\frac{3\cdot(1-\varepsilon_e)}{\Lambda}\right) \quad (18a)$$

with

$$\Lambda = -\beta_1^{-1}+(1-\varepsilon_e)+b_1\beta_3(1-\varepsilon_e)^{10/3}+b_2\beta_5(1-\varepsilon_e)^{14/3}+b_3\beta_3^2(1-\varepsilon_e)^{17/3}+b_4\beta_7(1-\varepsilon_e)^6+b_5\beta_3\beta_5(1-\varepsilon_e)^7+b_6\beta_9(1-\varepsilon_e)^{22/3} \quad (18b)$$

and

$$\beta_i = \frac{\alpha_{\text{part}}-1}{\alpha_{\text{part}}+(i+1)/i} \quad (18c)$$

The numerical coefficients for the b_i-coefficients appearing in Eq. (18b) are given in Table 1. The value of these coefficients depends upon the packing geometry and is different for the fcc-, bcc- and sc-case.

2.1.4. Torquato-approximations

Eq. (18) is accurate up to 9th order [26], but is very elaborate and hence difficult to use in practice. Fortunately, it was rigorously demonstrated by Torquato [15] that a highly accurate approximation to Eq. (18) could be obtained by truncating the solution after the 3rd order term and introducing the so-called three-point parameter ξ_2:

$$B = 2\gamma_{\text{eff}}(1+k') = \frac{2}{\varepsilon_T}\cdot\frac{1+2\beta_1(1-\varepsilon_e)-2\varepsilon_e\zeta_2{\beta_1}^2}{1-\beta_1(1-\varepsilon_e)-2\varepsilon_e\zeta_2{\beta_1}^2} \quad (19a)$$

with ξ_2 a given function of the particle fraction $(1-\varepsilon_e)$ [28]:

$$\zeta_2 = a_1(1-\varepsilon_e)\exp(a_2(1-\varepsilon_e)) \quad (19b)$$

A great asset of Eq. (19a) is that it also holds for a random packing of spheres, provided the appropriate a_i-coefficients are being used. These are summarized in Table 1 for the fcc-, bcc- and sc-case, as well as for random packing case. For a random packing with $\varepsilon_e = 0.4$, Eq. (19b) predicts a value of $\xi_2 = 0.11$. On the other hand, Miller and Torquato [29] have obtained that $\xi_2 = 0.13$. These values lie relatively close to each other, and anyhow do not produce a significant difference when applied in Eq. (19a) under most relevant conditions.

2.1.5. The Jeffrey- and Hashin-solution

One final EMT-expression considered here is linked to the work of Jeffrey [30] and that of Hashin [31], who have also solved the

Table 1
Values for the b_i-coefficients appearing in the exact Cheng and Torquato-expression (Eq. (18b)) and the a_i-coefficients appearing in the approximate Torquato-expression for spherical particles and cylindrical pillars (Eq. (19b)).

	Simple cubic	Body-centered cubic	Face-centered cubic	Random
a: Spherical particles				
b_1	1.30472	0.12930	0.07529	/
b_2	0.07232	0.25696	0.24195	/
b_3	−0.52895	−0.09881	0.05583	/
b_4	0.15256	0.01313	0.02311	/
b_5	−0.30667	0.05338	−0.05244	/
b_6	0.01045	0.00562	9.16×10^{-7}	/
a_1	7.181×10^{-3}	1.256×10^{-3}	8.670×10^{-4}	2.114×10^{-1}
a_2	7.816	7.759	7.962	-2.382×10^{-1}

	Square	Equilateral triangular	Random
b: Cylindrical pillars			
a_1	1.447×10^{-3}	2.151×10^{-5}	3.349×10^{-1}
a_2	7.871	1.082×10^{1}	-1.926×10^{-1}

random packed bed problem and have established a solution that is accurate up to order 3 [16]. Their expression can be rewritten as:

$$B = 2\gamma_{\text{eff}}(1+k') = \frac{2}{\varepsilon_T}\left[1 + 3\beta_1(1-\varepsilon_e) + 3\beta_1^2(1-\varepsilon_e)^2(1+2\delta\beta_1)\right] \tag{20}$$

with δ a tabulated fitting factor (see Table 1 of [30]) that varies only very weakly with α_{part} ($\delta = 0.22$ at $\alpha_{\text{part}} = 0$; $\delta = 0.21$ at $\alpha_{\text{part}} = 1$; $\delta = 0.25$ at $\alpha_{\text{part}} = +\infty$).

2.2. Implicit models

The most widespread used implicit model is the Landauer–Davis model [7,17,32]. In terms of the relative particle permeability α_{part}, and using the same transformations as in the previous section, the Landauer–Davis expression can be written as [4]:

$$B = 2\gamma_{\text{eff}}(1+k') = \frac{2\alpha_{\text{part}}}{\varepsilon_T}\left[A + \left(A^2 + \frac{2}{z-2}\cdot\frac{1}{\alpha_{\text{part}}}\right)^{1/2}\right] \tag{21a}$$

with

$$A = \frac{\left((z/2)\varepsilon_e - 1\right)\alpha_{\text{part}}^{-1} + \left((z/2)(1-\varepsilon_e) - 1\right)}{z-2} \tag{21b}$$

In this expression, the nearest neighbour interactions are represented by the so-called coordination number z. Often this number is taken as 6, but there is clear evidence that z can vary with the fraction of the void volume ε [17] and even with the intra-particle diffusion coefficient [5]. The reader should note that Eqs. (21a), (21b), originally introduced into the field in [4], are identical to the expressions used very recently in [10]. The equivalence can easily be checked by noting that $\varepsilon_e(1+k'') = \varepsilon_T(1+k')$ and by putting $z = 6$.

Implicit (or self-consistent) models however have an inherent weakness because they do not include any specific information regarding the spatial distribution of the included regions (spheres in the present case) [6]. Other implicit models, such as the differential effective-medium model first introduced by Bruggeman [33] are therefore not considered here.

2.3. Upper and lower limit expressions and the residence time weighted (RTW) model

Before proceeding, it is important to realize that every valid solution to the EMT should be bound [6,34] by the parallel-connection case (volume weighted-average), representing the upper permeability bound:

$$P_{\text{eff}} = \phi_m P_m + \phi_{\text{part}} P_{\text{part}} \tag{22}$$

and the series-connection case (harmonic average), representing the lower permeability bound:

$$\frac{1}{P_{\text{eff}}} = \frac{\phi_m}{P_m} + \frac{\phi_{\text{part}}}{P_{\text{part}}} \tag{23}$$

Applying the same transformation as in the two previous sections, Eqs. (22) and (23) become:

$$B = 2\gamma_{\text{eff}}(1+k') = 2\frac{\varepsilon_e + (1-\varepsilon_e)\alpha_{\text{part}}}{\varepsilon_T} \quad \text{(parallel-connection of resistances)} \tag{24}$$

$$B = 2\gamma_{\text{eff}}(1+k') = \frac{2}{\varepsilon_T}\cdot\frac{\alpha_{\text{part}}}{\varepsilon_e\alpha_{\text{part}} + 1 - \varepsilon_e} \quad \text{(series-connection of resistances)} \tag{25}$$

In Section 3, we will compare the EMT-expressions established in Sections 2.1 and 2.2 with these bounds, as well as with the traditionally employed parallel-zone or residence time weighted (RTW) model, used in nearly all studies of the B-term diffusion [1,2,35,36], and also consistently used in nearly all studies trying to measure the stationary phase diffusion coefficient $\gamma_s D_s/D_m$ [36,37]. Using the same notation as in Sections 2.1 and 2.2, this RTW-model can be written as:

$$B_{\text{RTW}} = 2\gamma_{\text{eff,RTW}}(1+k') = 2\frac{\varepsilon_e\gamma_e + (1-\varepsilon_e)\alpha_{\text{part}}}{\varepsilon_T} \tag{26}$$

The reader will note that Eq. (26) is very similar to Eq. (24), except for the γ_e-factor that is now appearing in the first term of the numerator. As such, the RTW-model can also be considered as a parallel-zone model, but with an empirical modification to find the correct B-term constant when the analytes only diffuse in the interstitial void space. Using Eqs. (2) and (4) and Eq. (S-18a) from the SM, Eq. (26) can also be reformulated into a form that can more easily be identified with the expressions for γ_{eff} and D_{eff} used in literature [1,2,24,36,38,39]:

$$\gamma_{\text{eff,RTW}} = \frac{D_{\text{eff}}}{D_m} = \frac{\varepsilon_e\gamma_e + (1-\varepsilon_e)\alpha_{\text{part}}}{\varepsilon_T(1+k')} = \frac{\varepsilon_e\gamma_e + (1-\varepsilon_e)\alpha_{\text{part}}}{\varepsilon_e(1+k'')} = \frac{\gamma_e + k''D_{\text{part}}}{1+k''} \tag{27}$$

For this purpose, it is also most convenient to replace α_{part} by its relation to γ_{mp} and $\gamma D_s/D_m$ (see Section 4.1).

2.4. Special case of cylinders

EMT-expressions have also been established for ordered and random cylinder packings [6]. The resulting expressions are very

Table 2
Expressions for γ_{eff} and B-term constant for the case of non-porous spheres and cylinders.

	Spheres	Cylinders
Maxwell	$\gamma_{np}=\gamma_e=\frac{1}{\tau^2}=\frac{2}{3-\varepsilon_e}$	$\gamma_{np}=\gamma_e=\frac{1}{\tau^2}=\frac{1}{2-\varepsilon_e}$
Rayleigh	$\gamma_{np}=\gamma_e=\frac{1}{\tau^2}=\frac{1}{\varepsilon_e}\left(1-\frac{3(1-\varepsilon_e)}{3-\varepsilon-0.392(1-\varepsilon_e)^{10/3}}\right)$	
Cheng and Torquato	$\gamma_{np}=\gamma_e=\frac{1}{\tau^2}=\frac{1}{\varepsilon_e}\left(1-\frac{3(1-\varepsilon_e)}{\Lambda}\right)$ with (b_i-constants given in Table 1a): $\Lambda=3-\varepsilon_e-\frac{3}{4}b_1(1-\varepsilon_e)^{10/3}-\frac{5}{6}b_2(1-\varepsilon_e)^{14/3}+\frac{9}{16}b_3(1-\varepsilon_e)^{17/3}-\frac{7}{8}b_4(1-\varepsilon_e)^6+\frac{15}{24}b_5(1-\varepsilon_e)^7-\frac{9}{10}b_6(1-\varepsilon_e)^{22/3}$	
Torquato	$\gamma_{np}=\gamma_e=\frac{1}{\tau^2}=\frac{2-\zeta_2}{3-\varepsilon_e(1+\zeta_2)}$	$\gamma_{np}=\gamma_e=\frac{1}{\tau^2}=\frac{1-\zeta_2}{2-\varepsilon_e(1+\zeta_2)}$
Landauer–Davis	$\gamma_{np}=\gamma_e=\frac{1}{\tau^2}=\frac{z-2/\varepsilon_e}{z-2}$	
Hashin	$\gamma_{np}=\gamma_e=\frac{1}{\tau^2}=\frac{1}{\varepsilon_e}\left(-0.5+1.5\varepsilon_e+0.75(1-\varepsilon_e)^2\left(1-\delta\right)\right)$	

similar to those for spherical particles, except for the value of some of the numerical constants appearing in the expressions. Using the same transformations as used in Section 2.1, the cylinder variant of the Maxwell-expression can be written as:

$$\beta_1=\frac{\alpha_{part}-1}{\alpha_{part}+1}, \tag{28}$$

and

$$B=2\gamma_{eff}(1+k')=\frac{2}{\varepsilon_T}\cdot\frac{1+\beta_1(1-\varepsilon_e)}{1-\beta_1(1-\varepsilon_e)} \tag{29}$$

Similar to the higher order extension that was obtained by Rayleigh for the spherical particle case, Barrer obtained an equivalent expression higher order expression for cylinders [4,17]. Again using the same approach as in Section 2.1, this can be written as:

$$\begin{aligned}B&=2\gamma_{eff}(1+k')\\&=\frac{2}{\varepsilon_T}\left[1+2(1-\varepsilon_e)\left[\beta_1^{-1}-(1-\varepsilon_e)+0.3\beta_1(1-\varepsilon_e)^4\right.\right.\\&\quad\left.\left.+0.13\beta_1(1-\varepsilon_e)^8\right]^{-1}\right]\end{aligned} \tag{30}$$

The high accuracy of the Barrer-model was already demonstrated in [4], where the model predictions coincided exactly with a set of numerically computed diffusion data in 2-D periodic arrays of fully porous cylinders.

The approximate Torquato-expression (Eq. (19a)) has a cylinder packing variant as well [15], which after adapting it to the permeability problem case, can be written as:

$$B=2\gamma_{eff}(1+k')=\frac{2}{\varepsilon_T}\cdot\frac{1+\beta_1(1-\varepsilon_e)-\varepsilon_e\zeta_2\beta_1{}^2}{1-\beta_1(1-\varepsilon_e)-\varepsilon_e\zeta_2\beta_1{}^2} \tag{31}$$

Similar to the difference between the cylinder and the sphere variant of the Maxwell-expression, the effect of the geometry here also only involves some minor changes in the numerical constants appearing in the expression. Using Eq. (31), care needs to be taken that also the appropriate a_i-constants appearing in the expression for the ξ_2-coefficient are used (see Table 1b).

2.5. Special case of non-porous particles

For the special case of non-porous particles, the expressions given in Section 2.1 greatly simplify. Since $\alpha_{part}=0$ in this case, it follows directly that:

$$\beta=-\frac{1}{2}\quad\text{(spherical particles)}\quad\text{and}\quad\beta=-1\quad\text{(cylindrical pillars)} \tag{32}$$

As a consequence, the general EMT-expressions given in Eqs. (16)–(21) considerably simplify. The resulting expressions are given in Table 2. Instead of relating them to the B-term constant as was done in Section 2.1, it was preferred to write the expressions in Table 2 in a form that directly yields γ_{np}. The subscript "np" is used to denote that the solution relates to a packing of non-porous particles (in which case we put $\gamma_{eff}=\gamma_{np}$). The γ_{np}-format has been preferred because one of the main applications of the non-porous particle case is the calculation of the obstruction factor inside the meso-porous zone of the particles. It is namely often assumed that the intra-particle obstruction factor can be calculated by representing the meso-porous zone as a packing of non-porous nano-spheres.

In this case, the different EMT-models can be used to predict the obstruction factor induced by the tortuosity of the pore space (γ_{np}). In many literature references, and also in the field of chemical engineering, γ_{np} is often also expressed as the meso-pore tortuosity γ, via the well established identity [9,38]:

$$\gamma_{np}=\frac{1}{\tau^2} \tag{33}$$

At this point, one should note that the "2" in the exponent for τ is omitted in some literature (e.g. [8,9]). This difference in notation has grown through the years, but has no mathematical consequences as it is only a matter of notation and definition.

In general, the diffusion in the meso-pore space is not only determined by its tortuosity, but also by the frequent collisions the analyte molecules make with the pore wall. To express this, the so-called diffusion hindrance factor $F(\lambda)$ is often introduced (λ is the ratio of the molecular diameter to the pore diameter and $F(\lambda)$ turns to unity when λ turns to zero). Traditionally, it is then assumed that the product of tortuosity and hindrance factor yields the true meso-pore obstruction factor γ_{mp} [3,38]:

$$\gamma_{mp}=\gamma_{np}F(\lambda)=\frac{F(\lambda)}{\tau^2} \tag{34}$$

With the aid of the expressions in Table 2, Eq. (34) can now be used to produce estimates for the meso-pore obstruction factor γ_{mp} used in expressions of the type given by Eq. (44) shown in Section 4.2 further on.

Returning to the column level, the γ_{np}-expressions presented in Table 2 also directly provide a value for the γ_e-factor appearing in the RTW-model (Eqs. (26), (27)), because the latter represents the obstruction factor in the interstitial void volume, and should thus correspond to the obstruction factor that would be obtained if the particles were non-porous.

With the above, we can now compare the different EMT-expressions for γ_{np} given in Table 2 with some of the literature

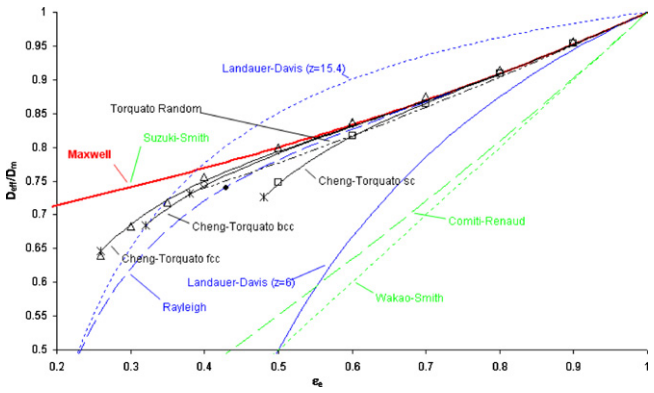

Fig. 3. Plot of $\gamma_{np} = \gamma_e = D_{eff}/D_m$ as a function of the packing density ε_e for the case of non-porous particles ($\alpha_{part} = 0$) using the expressions given in Section 2.5 and Table 2 (different model names are indicated on the graph). The data points (△ for fcc, ◊ for bcc and □ for sc) have been obtained via the numerical simulation study presented in part II. Also indicated (✳) are the close-packing limits for the random packing and the ordered fcc-, bcc- and sc-packing cases and an experimental data point (●) taken from [43]. (For interpretation of the references to color in this figure legend, the reader is referred to the web version of the article.)

correlations that are being used for γ_e and $1/\tau_{pz}^2$ (Fig. 3)

$$\gamma_{np} = \gamma_e = \frac{1}{\tau^2} = \frac{1}{\varepsilon_e + 1.5(1-\varepsilon_e)} \tag{35a}$$

(Suzuki and Smith [40])

$$\gamma_{np} = \gamma_e = \frac{1}{\tau^2} = \frac{1}{(1 - 0.5\ln\varepsilon_e)^2} \tag{35b}$$

(Comiti and Renaud [41])

$$\gamma_{np} = \gamma_e = \frac{1}{\tau^2} = \varepsilon_e \tag{35c}$$

(Wakao and Smith [42])

As a reference, the values for γ_{np} obtained in the numerical computation study presented in part II are given as well. As can be noted from Fig. 3 (both model curves coincide), and as can also be checked analytically, the Suzuki–Smith model is in fact identical to the Maxwell-based expression for γ_{np} (expressions: see Table 2). For high values of ε_e (non-touching spheres), the simple Suzuki–Smith and Maxwell-based expression provide an excellent approximation to any possible packing geometry. For smaller ε_e, approaching the closest-packing limit (denoted by ✳), the influence of geometry becomes more important, as can be noted from the fact that the curves representing the highest-order accuracy solution for the different packing geometries clearly diverge. The ordered bcc- and fcc-packing remain relatively close to each other, while the sc-packing yields more deviating γ_{np}-values. This reflects the fact that the geometries of the fcc- and a bcc-packing are much more similar than the sc-packing (see Fig. 2a–c).

As a point of reference, we also added the value of $\gamma_{np} = 0.74$ that was recently measured by Miyabe et al. for a packing with $\varepsilon_e = 0.43$ [43]. As can be noted, the agreement is very good and falls well within the range of experimental error margin.

The other two classical literature expressions (dashed and dotted green lines) clearly yield deviating values, most probably because the model is either too simplistic (Wakao–Smith [42]) or because it is based on hydrodynamic calculations (Comiti and Renaud [41]), which are known to produce a different tortuosity than diffusion calculations (simply because of the different phenomena they represent).

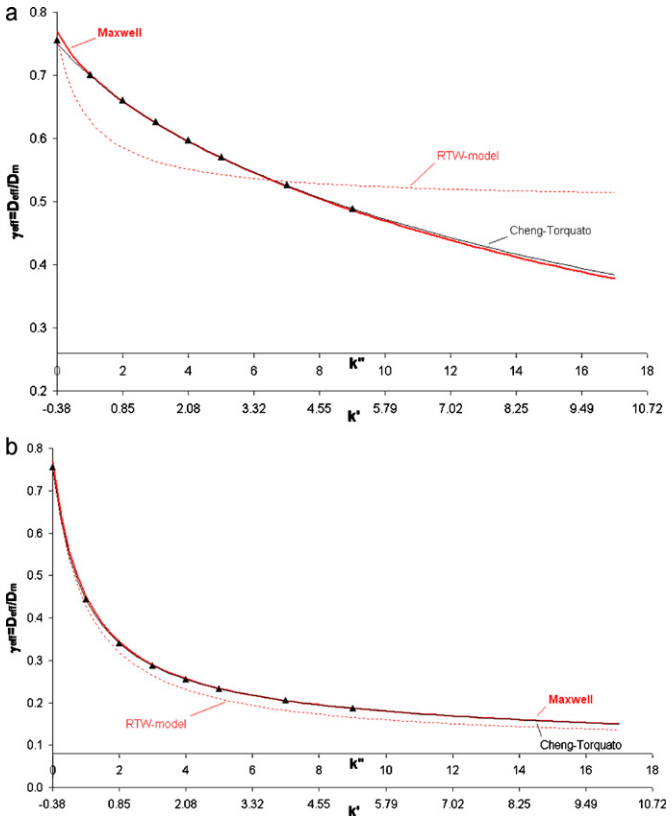

Fig. 4. Variation of D_{eff}/D_m as a function of k' and k'' for an fcc-packing with $\varepsilon_e = 0.4$ and (a) $D_{part}/D_m = 0.5$ and (b) $D_{part}/D_m = 0.1$. Model curves have been obtained via the Maxwell-based model (——), via the high-order accuracy Cheng–Torquato solution (——) and via the RTW-model (Eq. (26)) (- - - - - - -). The solid data points (▲) have been obtained in the study presented in part II. (For interpretation of the references to color in this figure legend, the reader is referred to the web version of the article.)

3. Characteristics of the different models and their sensitivity to the bed shape (fully porous case)

Fig. 4 shows how the D_{eff}/D_m-data predicted by the Maxwell-based expression (Eq. (16)) and by the highest-order accuracy Cheng–Torquato expression (Eq. (18)) evolve with k' and k'' in an fcc-packing with $\varepsilon_e = 0.40$ for two different values of the intra-particle diffusion coefficient D_{part}, one corresponding to a typically high ($D_{part}/D_m = 0.5$) and to a typically low value ($D_{part}/D_m = 0.1$). The results for two other D_{part}/D_m-values ($D_{part}/D_m = 0.25$ and $D_{part}/D_m = 0.05$) are given in the SM (as well as the results for an fcc-packing with a different external porosity: $\varepsilon_e = 0.35$). The solid data points again represent the values obtained via the computational study discussed in part II. The curve predicted by the RTW-model (Eq. (26)) is given as well.

A first observation that can be made from Fig. 4 concerns the general steepness of the presented D_{eff}-curves, for which it can be concluded that, the lower the D_{part}-value, the steeper the relation between D_{eff} and the retention factors k' and k''. This is in agreement with one's physical expectations. A higher retention factor namely implies that the analytes spend more time in the particles, so that their effective diffusion is more affected by D_{part}. As a consequence, and since all curves need to depart from the same γ_e-point at $k'' = 0$, D_{eff} will decrease more sharply with increasing k' or k'' when D_{part} is low than when D_{part} is high.

Despite its enormous simplicity compared to the other EMT-models, and despite the dilute suspension assumption it is based on, it is also striking to note how well the Maxwell-based expression (red curves in Fig. 4) follows the trend of the highest-order

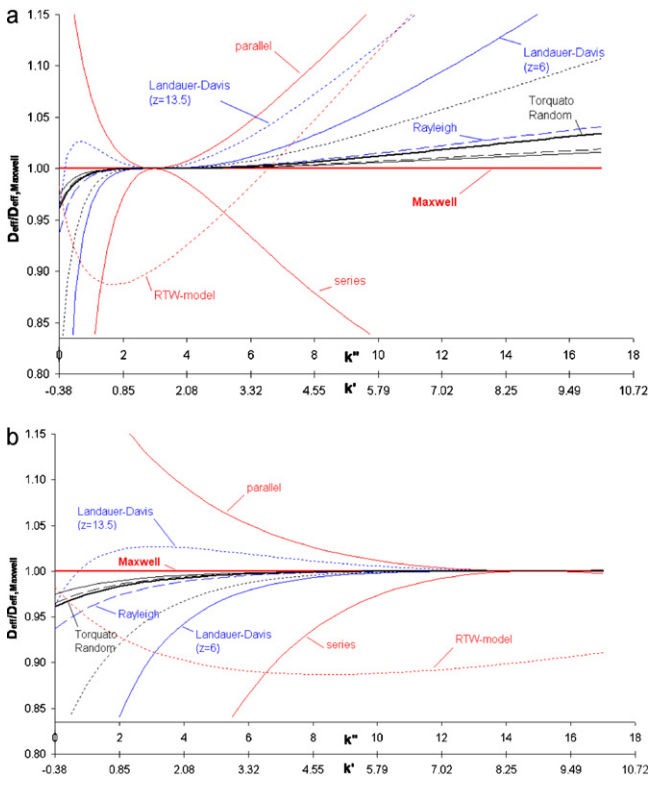

Fig. 5. Plot of $D_{eff}/D_{eff,Maxwell}$ ("Maxwell-plot") for different EMT-models and the RTW-model for $\varepsilon_e = 0.4$ and for (a) $D_{part}/D_m = 0.5$ and (b) $D_{part}/D_m = 0.1$. The different curves pertain to the different considered models: Maxwell (——), Cheng–Torquato fcc (——), bcc (— —), sc (- - - - - - -), Landauer–Davis $z = 6$ (——), z = best fit (- - - - - - -), Rayleigh (— —), Torquato Random (——), the series and parallel limits (——) and the RTW-model (- - - - - - -). (For interpretation of the references to color in this figure legend, the reader is referred to the web version of the article.)

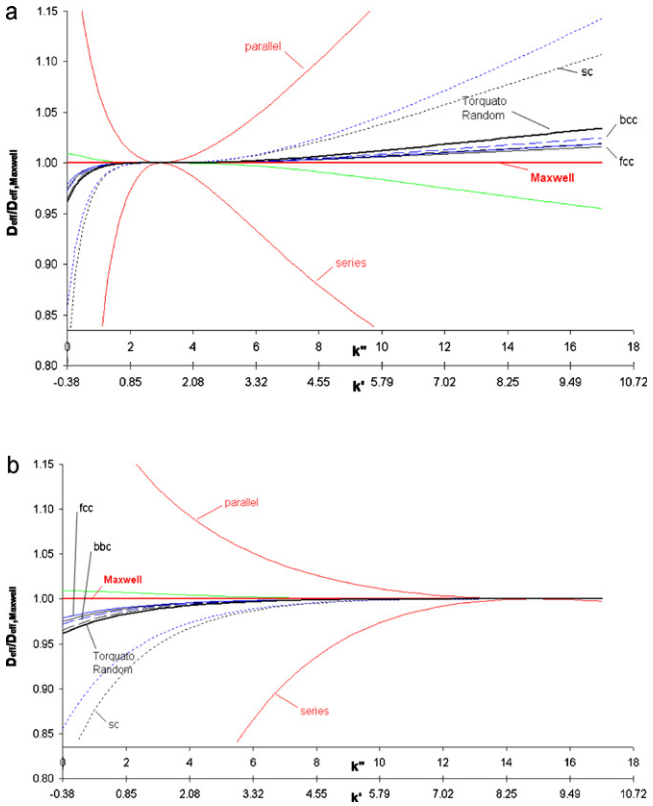

Fig. 6. Plot of $D_{eff}/D_{eff,Maxwell}$ ("Maxwell-plot") for different EMT-models for $\varepsilon_e = 0.4$ and for (a) $D_{part}/D_m = 0.5$ and (b) $D_{part}/D_m = 0.1$. The different curves pertain to the different considered models: Maxwell (——), Cheng–Torquato fcc (——), bcc (— —), sc (- - - - - - -), Torquato fcc (——), bcc (— —), sc (- - - - - - -), Torquato Random (——), the series and parallel limits (——) and Hashin (——). (For interpretation of the references to color in this figure legend, the reader is referred to the web version of the article.)

accuracy EMT-expressions established by Cheng and Torquato (Eq. (18), black curves). The agreement with the data points of the computational fluid dynamics study discussed in part II is also excellent. The RTW-model on the other hand completely fails in the $D_{part}/D_m = 0.5$-case, and also clearly deviates from the true solution in the $D_{part}/D_m = 0.1$-case. All observations described above also hold for a bcc-packing with $\varepsilon_e = 0.40$ (data not shown).

To investigate the mutual differences between the different models in more detail, and trying to find an explanation for the excellent accuracy of the simple Maxwell-expression, it is convenient to represent the D_{eff}-data as a plot of $D_{eff}/D_{eff,Maxwell}$ (see Figs. 5 and 6). This type of plot, further on referred to as the "Maxwell-plot", is obtained by calculating D_{eff} via any of the expressions established in Sections 2.1 and 2.2 and subsequently dividing the result by the D_{eff}-value obtained via the Maxwell-expression. This transforms the curved red lines shown in Fig. 4 into a flat horizontal line with $D_{eff}/D_{eff,Maxwell} = 1$. As a consequence, the differences between the different models are considerably magnified.

To understand the observed trends in Figs. 5 and 6, a key role is played by the upper and lower bound expressions given by Eqs. (24), (25), and respectively representing the series- (see Fig. 1c) and the parallel-connection case (see Fig. 1d). According to the EMT, all physically possible solutions for D_{eff} should be situated between these two limiting diffusion regimes. Intuitively, this can readily be understood by noting that, in the general case, the diffusion is composed out of parallel- as well as serially-connected trajectories (resp. represented by trajectory 1 and 2 in Fig. 1a). Obviously, the serially-connected case (Fig. 1c) always produces the lowest effective diffusion rate since all diffusing molecules have to successively pass through the rate limiting low diffusion zones (dark region), whereas in the pure parallel case (Fig. 1d), the analytes can always follow an unobstructed path in the high diffusion zone (light regions) which obviously corresponds to the highest possible effective diffusion rate.

As can be noted from Figs. 5 and 6, all EMT-expressions from Sections 2.1 and 2.2 clearly obey the upper- and lower bound rule and are situated between the series- and parallel-connection limit. The RTW-model on the other hand clearly disobeys this rule, thus pointing at its physical invalidity. In hindsight, the latter is not surprising, because the RTW-model is based on the (clearly erroneous) assumption that the low and high diffusion area arranged in purely parallel running strips, and then empirically corrected with a γ_e-factor to ensure that the correct γ_{eff}-obstruction factor is obtained at $k' = 0$ or $k'' = 0$.

An important characteristic of the upper and lower bound expressions for the parallel- and series-connection case that can be noted from Fig. 5 is that they completely diverge in the low and high retention end of the curves, but converge and actually coincide for some intermediate value of the retention factor. This is clearly the case in Figs. 5a and 6a ($D_{part}/D_m = 0.5$). In Figs. 5b and 6b ($D_{part}/D_m = 0.1$) this convergence point is situated at the outmost right side of the plot. It can however be verified that the curves again diverge when proceeding further to the right (see also discussion further on below).

Considering now that all EMT-expressions directly depend on the relative permeability α_{part}, it should be noted that this relative permeability varies in Figs. 5a and 6a from a value well below unity ($\alpha_{part} = 0$ at $k'' = 0$, see Eq. (12)) to a value well above unity ($\alpha_{part} = 6$

if k'' = 18 and D_{part}/D_m = 0.5 and ε_e = 0.4, see Eq. (12)). Subsequently equating the expressions for the parallel- and the series-connection bounds (Eqs. (24), (25)) yields:

$$B_{series} = B_{parallel} \Leftrightarrow \varepsilon_e + (1-\varepsilon_e)\alpha_{part} = \frac{\alpha_{part}}{\varepsilon_e \alpha_{part} + 1 - \varepsilon_e} \quad (36)$$

It can easily be verified that this equation has one and only one solution, simply given by α_{part} = 1. In other words, the upper and lower bound solution meet each other when the particles have the same permeability as the surrounding medium, in full agreement with one's physical expectations. Since the α_{part} = 1-condition corresponds to the case wherein the dark and light regions in Fig. 1a and c–d have the same permeability, it should indeed not make any difference whether the dark regions are aligned in parallel or in series or are arranged as an array of spherical inclusions. In terms of the particle-based retention equilibrium constant K_{part}, it can be noted from Eq. (11) that the α_{part} = 1-condition corresponds to the case wherein K_{part} has just achieved the right value to make the product of K_{part} and D_{part} exactly equal to D_m. In general terms, the above can thus be summarized as:

$$\text{Effective permeability independent of geometry} \Leftrightarrow \alpha_{part} = 1 \quad (37)$$

For the parameter values considered in Figs. 5b and 6b (D_{part}/D_m = 0.1), the α_{part} = 1-condition is only achieved at k'' = 15, hence explaining why the convergence point is situated so far to the right.

With the above we can now better understand the general trends observed in Figs. 5 and 6 (and also those in Figs. S-2 to S-6 of the SM). Taking the exact Cheng–Torquato model for random packed beds as the reference (thick black line), because this is by far the geometry with the highest practical relevance, it can clearly be noted that the two different considered Landauer–Davis expressions (one with z = 6 and one with z = best-fit value) deviate significantly from the exact Cheng–Torquato solution. Considering the assumptions underlying the Landauer–Davis (LD) model, this should not come as a surprise. Implicit or self-symmetrical models such as the LD-model namely lack any direct relation to the geometry of the bed, and treat the column as a symmetrical binary medium [6]. The latter fact, implying that the LD-model is based on the assumption that the low diffusivity in the particle zone and the high diffusivity in the interstitial void zone are interchangeable, is clearly in conflict with the physical reality. The LD-model with z = 6 obviously fits less well than the one with the best-fit z-value. However, the better fit of the latter is in practice not very helpful since there are no rules to predict the required value of z.

The Maxwell-model (red line), and especially its higher order accuracy variant (the Rayleigh model), represented by the dashed blue line, follow the trend of the random packing curve much closer. This is in agreement with one's physical expectations, since both models are fully explicit, directly taking the spherical shape of the particles into account, and do not rely upon the phase symmetry-assumption as does the LD-model.

Fig. 6 can be used to assess the differences between the highest-order accuracy solutions for the fcc-, bcc- and sc-arrangement established by Cheng and Torquato (Eq. (18)) and the three-point approximation of Torquato (Eq. (19a)). As can be noted, the latter (blue curves) approximates the highest-accuracy solution of Cheng and Torquato (black curves) very well. Given the Torquato-approximation is much simpler to use, it offers a good compromise between accuracy and practical utility. The sc-case on the other hand produces a D_{eff}-behaviour that is significantly different from the fcc- and bcc-packing case, in full agreement with the fact that the packing geometry of the fcc- and the bcc-case are very similar, whereas the sc-packing case contains much larger void spaces. This can be witnessed from Fig. 2, and is also in agreement with the fact that the maximal packing density of the sc-case ($\varepsilon_{e,cp}$ = 0.48) strongly deviates from the bcc- and the fcc-case, for which respectively $\varepsilon_{e,cp}$ = 0.32 and $\varepsilon_{e,cp}$ = 0.26.

Yet another observation that can be made from Fig. 6 is that the random packing case displays a D_{eff}-behaviour that lies somewhere intermediate between the fcc-, bcc- and sc-case. This makes perfect sense, since a random packing inevitably consists of a combination of fcc-, bcc- and sc-like regions [14]. The random packing solution lies closer to the fcc- and the bcc-case than to the sc-case. The latter is in full agreement with the fact that the sc-packing geometry is much less stable and sc-regions therefore seldom form when packing a bed.

In a more quantitative way, it can be concluded from Figs. 5 and 6 that the difference between the Maxwell-curve and the random packing curve is everywhere less than 4%. Depending on the intra-particle diffusion rate, the Maxwell-curve is even accurate to within 1% in the range of $0.1 < k' < 5.2$ for the case of D_{part}/D_m = 0.5 (Fig. 6a) and in the range of $1.6 < k' < 30$ for the case of D_{part}/D_m = 0.1 (Fig. 6b, upper limit value is not shown on graph but was verified analytically). Similar values are obtained for the other considered D_{part}/D_m-cases. In fact, the following general trend can be discerned when comparing all considered cases: the smaller D_{part}/D_m, the broader the range of k'-values wherein the Maxwell-model approximates the random packing geometry to within 1%. This implies that for most relevant cases, the Maxwell-solution already provides an excellent approximation. Given the relative simplicity of the Maxwell-solution this is a very fortunate situation.

Another observation that can be made from Fig. 5 is that the difference between Torquato's approximate three-point solution and the highest-order accuracy result of Cheng and Torquato (respectively represented by the black and blue curves) is very small (maximally 1% if ε_e = 0.4 and 1.4% if ε_e = 0.35) for the fcc- and the bcc-case. The difference is significantly larger for the sc-case, but this type of packing is anyhow not very relevant for real packed bed columns.

The most important deviation between the different models (thus reflecting the sensitivity to the exact geometry of the packing) for chromatographic applications clearly occurs in the k'' = 0-limit (outer left hand side of the graphs), i.e., the case of a packing of fully solid particles. This limiting case has however already been discussed in Section 2.5 and Fig. 3.

4. Formulation of the EMT-expressions in terms of the microscopic material and physicochemical parameters

To effectively use the EMT-expressions discussed in the previous sections to calculate the value of the B-term constant and γ_{eff}, the relation between the externally observed intra-particle diffusion coefficient D_{part} (appearing in all EMT-models via β_1 and α_{part}) and the microscopic material and physicochemical parameters needs to be known as well.

4.1. Effect of the presence of a solid core

Zooming in on the microscopic details of the particle (Fig. 1b), the first obvious material parameter that needs to be taken into account when considering the general case wherein the particles might contain a central solid core, is the relative core diameter ρ ($\rho = d_{core}/d_{part}$) [44].

In this case, it is also important to distinguish between ε_{pz} and ε_{part} [10]. Whereas ε_{pz} is the fraction occupied by the non-retained species and the mobile phase in the meso-porous zone (either full particle or porous-shell), ε_{part} represents the same fraction but now expressed on a whole-particle basis. The latter hence accounts for the fact that the solid core occupies a significant fraction of the par-

ticles that cannot be accessed by the mobile phase. Both quantities are related by [44]:

$$\varepsilon_{part} = \left(1-\rho^3\right)\varepsilon_{pz} \quad \text{(spheres)} \tag{38a}$$

$$\varepsilon_{part} = \left(1-\rho^2\right)\varepsilon_{pz} \quad \text{(cylinders)} \tag{38b}$$

To properly represent the effect of the solid core, it is also important to distinguish between D_{pz} and D_{part}. With reference to Fig. 1b, D_{pz} is the symbol we use for the diffusion coefficient experienced by the species once they entered the meso-porous zone (entire particle in case of fully porous particle; shell layer in case of a porous-shell particle). On the other hand, D_{part} is the externally observed intra-particle diffusion coefficient. For a fully porous particle, the whole particle consists of the same meso-porous zone, so that simply:

$$D_{part} = D_{pz} \quad \text{(fully porous particle only)} \tag{39}$$

For a porous-shell particle, however, an external observer experiences an intra-particle diffusion coefficient lumping the diffusion in the meso-porous zone (shell layer) with the 100% obstruction introduced by the solid core.

In this case, the column can in fact be considered as a ternary medium, filled with spheres containing a concentric shell of a material with a different permeability than that of the central core. For the case of thermal and electrical conductivity, Hashin and Shtrikman, could show that such concentrically coated spherical particles can be represented by a uniform particle with an effective conductivity (or permeability in the terminology of the present study) given by [19,31]:

$$P_{eff,part} = \langle P\rangle - \frac{(P_2-P_1)^2\phi_1\phi_2}{\langle\overline{P}\rangle + (n-1)P_1} \tag{40a}$$

with

$$\langle P\rangle = \phi_1 P_1 + \phi_2 P_2 \quad \text{and} \quad \langle\overline{P}\rangle = \phi_1 P_2 + \phi_2 P_1 \tag{40b}$$

and

$$n = 2\,\text{(cylinders)} \quad \text{or} \quad n = 3\,\text{(spheres)} \tag{40c}$$

$P_2 = 0$ for the presently considered case of a non-porous core. Noting further that there is no preferential solubility between phase 1 and 2 so that $P_1 = D_1 = D_{pz}$ and $P_{eff,part} = D_{part}$, and also considering that $\phi_2 = \rho^3$ for spheres and $\phi_2 = \rho^2$ for cylinders ($\phi_1 = 1-\phi_2$), Eq. (40) can be rewritten as:

$$D_{part} = \frac{2}{2+\rho^3}D_{pz} \quad \text{(spherical particle case)} \tag{41}$$

$$D_{part} = \frac{1}{1+\rho^2}D_{pz} \quad \text{(cylindrical pillar case)} \tag{42}$$

When ρ turns to zero (no core), Eqs. (41) and (42) reduce to Eq. (39), as expected.

Eq. (40) is mathematically exact and generally valid for any value of ρ and also for any type of particle or pillar arrangement (ordered and random packings) [19,31]. This hence also holds for Eqs. (41) and (42).

Since the EMT-expressions for B and γ_{eff} (via β_1) are based on relative permeabilities rather than on diffusivities, it is convenient to establish a relation between the relative permeability of the particle (α_{part}) and that of the porous zone (α_{pz}). As shown in the SM, this relation is given by:

$$\alpha_{part} = \frac{2(1-\rho^3)}{2+\rho^3}\alpha_{pz} \quad \text{(spherical particles)} \tag{43a}$$

or

$$\alpha_{part} = \frac{1-\rho^2}{1+\rho^2}\alpha_{pz} \quad \text{(cylindrical pillars)} \tag{43b}$$

For particles without solid core, $\rho = 0$, and Eqs. (43a) and (43b) reduce to:

$$\alpha_{part} = \alpha_{pz} \quad \text{(fully porous particles)} \tag{43c}$$

in full agreement with Eq. (39).

4.2. Expressions for the diffusion coefficient D_{pz} and the relative permeability α_{pz} of the porous zone

As can be noted from the above sections, the relative permeability α_{pz} of the meso-porous zone is the basic parameter that is needed to calculate B. In the present contribution, two different approaches to calculate the value of α_{pz} are considered. These are discussed in the two sections below.

4.2.1. Expressions based on the residence time weighted addition of diffusion rates

The first approach is based on the assumption that the effective diffusion in the meso-porous zone can be calculated by making a residence time weighted addition of the diffusion experienced by the analytes while moving through the meso-pores in the non-retained state (during which $D = \gamma_{mp}D_m$) and that experienced while being retained on or in the stationary phase (during which $D = \gamma_s D_s$). This is the assumption that is traditionally made in literature [1,38], and corresponds to the assumption that the diffusion in the mobile phase in the meso-pores and that in or on the stationary phase occurs in parallel. As shown in the SM, this assumption leads to the following expression for D_{pz}:

$$D_{pz} = \frac{\varepsilon_{pz}\gamma_{mp}D_m + (1-\varepsilon_{pz})K_{A,pz}\gamma_s D_S}{\varepsilon_{pz} + (1-\varepsilon_{pz})K_{A,pz}} \tag{44}$$

To the best of our knowledge, this expression has for the first time been introduced by Knox [1] and Stout and De Stefano [2]. As shown in the SM, Eq. (44) directly leads to:

$$\alpha_{pz} = \varepsilon_{pz}\gamma_{mp} + (1-\varepsilon_{pz})K_{A,pz}\frac{\gamma_s D_S}{D_m} \tag{45}$$

The reader will note that the right hand side of Eq. (45) is identical to the expression for the Ω-factor introduced in [10,24,35,38]. Similarly, the effective permeability of the mobile zone ($P_{pz} = D_m\alpha_{pz}$) that is obtained by multiplying both sides of Eq. (45) with the molecular diffusion coefficient D_m is equivalent to the expressions for $\Omega{\cdot}D_m$ and D_e traditionally used in the recent general rate model literature [23,24,38,44–46]. It is however clear from the derivation leading to the establishment of Eqs. (S-27) and (S-25) in the SM that both Ω and D_e represent a permeability and not a diffusivity.

In some recent literature [45], the stationary phase obstruction factor (γ_s) has already been incorporated into the D_s-value that is being used or reported. In the present study, it has been preferred here to keep the $\gamma_s D_s$-notation to emphasize the difference with the D_{pz}-model established in Section 4.2.2.

Eqs. (44) and (45) can also be readily expressed in terms of the retention factors k' or k''. The resulting expressions are given by Eqs. (S-28) and (S-29) of the SM.

4.2.2. Expressions directly derived from the EMT

As already mentioned, Eq. (44) is directly based on the parallel-zone assumption, wherein the meso-porous zone is viewed as a parallel bundle of cylindrical meso-pores, albeit with a given tortuosity. However, the meso-porous zone is often also imagined as a sintered packing of nano-spheres. In this case, the meso-porous zone could be imagined as a ternary medium, consisting of the mobile phase liquid, filling the meso-pores, the impermeable silica particles, and a stationary phase layer covering the impermeable

silica. In this case, one can again use the Hashin–Shtrikman solution for ternary media already used in Section 4.1. Although the representation as a packing of spheres or cylinders is for most meso-porous materials perhaps only a very crude approximation (except for those particles that really consist of an agglomeration of solid nano-spheres), it nevertheless seems worthwhile to consider it and study the difference with the pure parallel-zone model, which is obviously also only an approximation of the reality.

To apply the Hashin–Shtrikman approach used in Section 4.1, the meso-porous zone should be represented (see also part 1.2.2 of the SM) as a binary medium consisting of (i) the meso-pores filled with mobile phase (occupying a fraction ε_{pz} and having a permeability $P = P_m$), and (ii) the "solid" zone composed of the solid silica and the stationary phase material (occupying a fraction $1-\varepsilon_{pz}$ and having a permeability $P = P_s$). Subsequently, α_{pz} can be defined as the ratio of the permeability governing the two different zones. Considering then the spherical particle case, and using the simple Maxwell-model (cf. Eq. (16)), we readily obtain:

$$\alpha_{pz} = \frac{P_{pz}}{P_m} = \frac{1+2\beta_1(1-\varepsilon_{pz})}{1-\beta_1(1-\varepsilon_{pz})} \tag{46}$$

with

$$\beta_1 = \frac{\alpha_{sol}-1}{\alpha_{sol}+2} \tag{47}$$

wherein α_{sol} is the relative permeability of the solid zone. Subsequently depicting this solid zone as a solid impermeable core with a uniform coating of stationary phase material with diffusion coefficient D_s, and defining ρ_{sol} as:

$$\rho_{sol} = d_{silica}/(d_{silica}+2\delta_s) \tag{48a}$$

or as

$$\rho_{sol} = \sqrt[3]{V_{silica}/(V_{silica}+V_s)} \tag{48b}$$

we can write in analogy with Eq. (43) that

$$\alpha_{sol} = \frac{2(1-\rho_{sol}^3)}{2+\rho_{sol}^3}\alpha_s \tag{49}$$

wherein α_s is the relative permeability of the pure stationary phase material (i.e., assuming there is no obstruction factor), which in analogy with Eq. (11), can be calculated as:

$$\alpha_s = \frac{K_{A,pz}D_s}{D_m} \tag{50}$$

As shown in the SM, the expression for α_{pz} can readily be transformed into an expression for the D_{pz}, yielding:

$$D_{pz} = \frac{1+2\beta_1(1-\varepsilon_{pz})}{1-\beta_1(1-\varepsilon_{pz})}\cdot\frac{D_m}{\varepsilon_{pz}+(1-\varepsilon_{pz})K_{A,pz}} \tag{51}$$

If desired, Eqs. (46) and (51) can also be readily expressed in terms of the retention factors k' or k''. The resulting expressions are given by Eqs. (S-32) and (S-33) of the SM.

In case a packing of cylindrical pillars would be a more appropriate representation of the reality, the factors 2 appearing in Eq. (46) should be turned into a factor 1 (in analogy with Eq. (29)) and the power of 1/3 and 3 appearing in Eqs. (48b) and (49) should be replaced by a power of 1/2 and 2. It is also possible to use some of the more elaborate EMT-expressions that can be found in literature or in Section 2.1 to replace the right hand side of Eq. (46). One particularly interesting solution would be the use of Eq. (19a), in combination with the ξ_2-values that prevail in packings of partially overlapping spheres [47], as this could in some cases constitute a closer representation of the real geometry of the meso-porous space.

Fig. 7 compares the evolution of D_{pz}/D_m with $K_{A,pz}$ predicted by the RTW-model (Eq. (44)) and that predicted by the EMT-approach

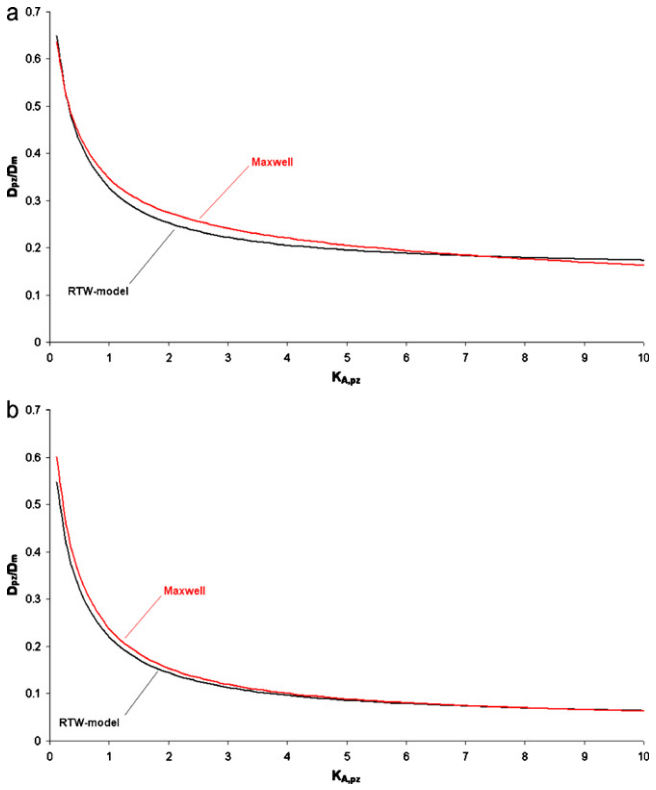

Fig. 7. Plot of D_{pz}/D_m versus $K_{A,pz}$ predicted by the RTW-model (Eq. (26)) (——) and by the Maxwell-based expression (Eq. (16)) (——) for (a) $D_s/D_m = 0.5$ and (b) $D_s/D_m = 0.1$. Parameter assumptions: $\varepsilon_e = 0.4$; $\varepsilon_{pz} = 0.4$; $\varepsilon_T = 0.64$; $\rho_{sol} = 0.85$; $\gamma_{mp} = 0.8$ and $\gamma_s = 0.5$ for case (a) and $\gamma_{mp} = 0.7$ and $\gamma_s = 0.7$ for case (b). (For interpretation of the references to color in this figure legend, the reader is referred to the web version of the article.)

(Eq. (46)). As can be noted, it is always possible to select a value for γ_{mp} and γ_s such that the RTW-model yields a curve that runs close to the Maxwell-based prediction (see figure caption for γ_{mp} and γ_s-values). The difference appears to be smaller than the typical experimental error margin, so that it will be difficult to differentiate between both models from peak parking measurement alone.

It should also be noted that, as opposed to the RTW-based model for D_{pz} (Eq. (44)), the EMT-based model for D_{pz} (Eq. (51)) no longer requires estimation of the values of γ_{mp} and γ_s, as these come "for free" with the EMT-approach, i.e., the effect of the obstruction is automatically incorporated in the obtained value for D_{pz}.

5. Reverse calculation: determining D_{part}, D_{pz}, γ_{mp} and $\gamma_s D_s/D_m$ from a measured set of *B*- or γ_{eff}-values

Apart from modelling and predicting the *B*-term constant of the van Deemter-curve, the EMT-expressions established in Section 2 should also allow to make the reverse calculation, i.e., determining the value of D_{pz} (and D_{part}) and/or the value of the microscopic intra-particle diffusion parameters γ_{mp}, $\gamma D_s/D_m$ and D_s starting from a measurement of D_{eff} or from an experimentally determined *B*-term constant value.

In this type of reverse calculation, the left hand side of Eqs. (16)–(20) is known and one is interested in finding the value of α_{part}. Although Eqs. (16)–(20) can of course always be solved numerically for α_{part}, it is much more convenient if α_{part} could be calculated via an explicit analytical expression. Since they are respectively limited to a 1st- and 2nd-order dependency on α_{part}, such an analytical expression must exist for the Maxwell-based (Eq. (16)) and the Torquato-based expression (Eq. (19a)).

Starting from the measured value of either B or γ_{eff}, and first considering the Maxwell-based expression for spheres (Eq. (16)) and cylinders (Eq. (29)), it is relatively straightforward to isolate β_1 and subsequently use the link between B and γ_{eff} given in Eq. (4) to arrive at:

$$\beta_1 = \frac{1}{1-\varepsilon_e}\cdot\frac{B\varepsilon_T - 2}{B\varepsilon_T + 4}\,(\text{spheres}) \quad \text{or}$$

$$\beta_1 = \frac{1}{1-\varepsilon_e}\cdot\frac{B\varepsilon_T - 2}{B\varepsilon_T + 2}\,(\text{cylinders}) \tag{52}$$

Desiring a higher accuracy (especially needed if the measurement is situated in the small k' region and or non-porous particle case), and switching to the Torquato-based expression (Eq. (19a) for spheres), it is somewhat more cumbersome to isolate β_1. Nevertheless, since the expression is only quadratic in β_1, a directly applicable analytical expression can still be obtained:

$$\beta_1 = \frac{(\varepsilon_e-1)(4+B\varepsilon_T) + \sqrt{(4+B\varepsilon_T)^2(1-\varepsilon_e)^2 + 8\varepsilon_e\zeta_2(B\varepsilon_T-2)^2}}{4\varepsilon_e\zeta_2(B\varepsilon_T-2)}\,(\text{spheres}) \tag{53a}$$

The negative root of the quadratic equation can be discarded since this always produces a value that lies outside the range $-0.5 \le \beta_1 \le 1$. Inserting such a value into Eq. (54) established further on would yield a negative value for α_{part}, which is of course physically invalid.

Similarly, we can also transform the cylinder-variant of the Torquato-based expression (Eq. (31)). This then yields:

$$\beta_1 = \frac{(\varepsilon_e-1)(2+B\varepsilon_T) + \sqrt{(2+B\varepsilon_T)^2(1-\varepsilon_e)^2 + 4\varepsilon_e\zeta_2(B\varepsilon_T-2)^2}}{2\varepsilon_e\zeta_2(B\varepsilon_T-2)}\,(\text{cylinders}) \tag{53b}$$

Once β_1 is known, it is straightforward to calculate the value for the relative particle permeability α_{part} by inverting either Eq. (13) or (28), respectively yielding:

$$\alpha_{part} = \frac{1+2\beta_1}{1-\beta_1}\,(\text{spheres}) \quad \text{or} \quad \alpha_{part} = \frac{1+\beta_1}{1-\beta_1}\,(\text{cylinders}) \tag{54}$$

Subsequently using the relation between α_{part} and D_{part} (via Eq. (12)), it is found that:

$$\frac{D_{part}}{D_m} = \frac{1-\varepsilon_e}{\varepsilon_e\cdot k''}\alpha_{part} = \frac{1-\varepsilon_e}{(1+k')\varepsilon_T - \varepsilon_e}\alpha_{part} \tag{55}$$

from which it is straightforward to obtain D_{pz} via the generally valid Eq. (41) (spherical particle case) or Eq. (42) (cylindrical pillar case), or by simply recognizing that $D_{pz} = D_{part}$ in the case of fully porous particles. From the known value of D_{pz}, the expressions given in Section 4.2 and in Sections 1.2.1 and 1.2.1 of the SM can subsequently be used to determine the microscopic intra-particle diffusion parameters γ_{mp}, $\gamma_s D_s/D_m$ and D_s.

To compare the accuracy with which the value of D_{part} (or D_{pz}) can be determined from a set of peak parking or B-term constant measurements, Fig. 8 compares the D_{part}-values obtained when using the Maxwell-model starting from a set of B-term constants generated using the random packing variant of the Torquato-model (Eq. (18)). These values are compared with the values for D_{part} obtained by starting from the same B-term constant value but by using the RTW-model. To simplify the calculation, it was assumed that D_{part} is independent of the retention factor, but it can be verified that this simplification does not take away from the generality of the obtained conclusions. As can be noted from Fig. 8, the Maxwell-model (Eq. (52)) produces D_{part}-values that approximate the true D_{part}-values (represented by the horizontal black line). This implies that the relatively simple expression given in Eq. (52) is in most cases sufficiently accurate to reliably estimate the D_{part}-value from a series of B-term constant or γ_{eff}-measurements (except for the practically irrelevant cases with $k'' < 1$). In agreement with the observations already made in [5], the RTW-based predictions deviate much more strongly, despite the apparent good fit that can be obtained in the small D_{pz}-case (see Fig. 4b). The RTW-model clearly induces a false monotonous trend in the observed D_{part}-values, as these appear to decrease with increasing retention, whereas the true value used to produce the B-term constant data was assumed to be independent of k' (horizontal black line data).

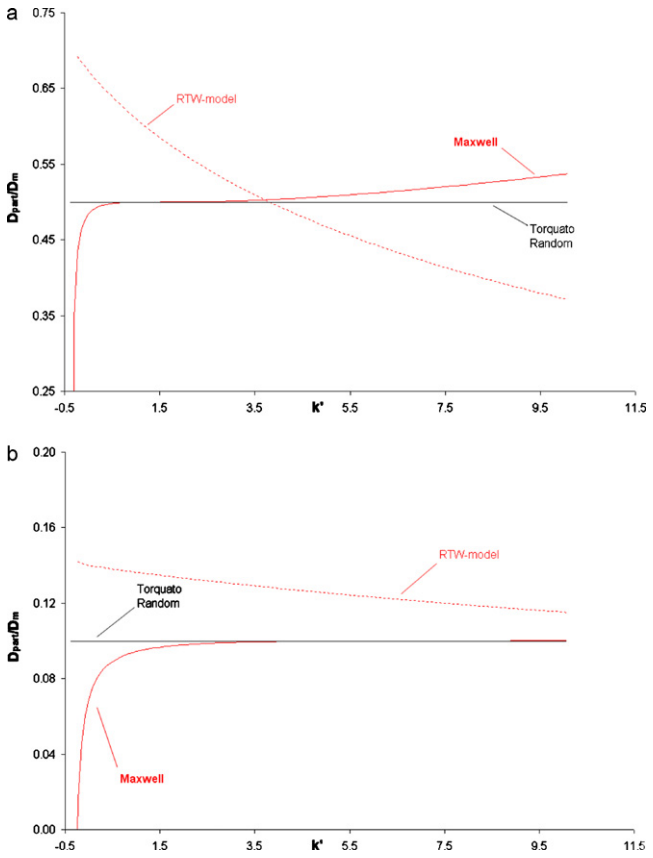

Fig. 8. Plot of the D_{part}/D_m-values obtained using the inverse Torquato-expression (Eq. (53)) (——), the inverse Maxwell-expression (Eq. (52)) (——) and the RTW-model (- - - - - - -) starting from a set of B-term coefficients generated via Torquato's random packing model with known and fixed D_{part} (represented by the flat horizontal line). Data are plotted versus the phase retention factor k'. (a) $D_{part}/D_m = 0.5$ and (b) $D_{part}/D_m = 0.1$. (For interpretation of the references to color in this figure legend, the reader is referred to the web version of the article.)

6. Conclusions

A variety of Effective Medium Theory (EMT) expressions exist in the literature on the effective electrical and thermal conductivity of packings of spheres and cylinders. Using the permeability analogue of the diffusion and partitioning processes occurring in a chromatographic column, these expressions can be transformed into expressions predicting the B-term band broadening in a very accurate way. These predictions are much more accurate than those obtained with the traditionally employed residence time weighted (RTW) expressions of the type shown in Eqs. (26) and (27), because these are based on the (erroneous) assumption that the concentration gradients inside and outside the particles are independent of each other. As a consequence, the RTW-expressions even violate one of the basic rules of the EMT by breaking through the upper and lower limits for the effective diffusion.

Within the broad family of EMT-models, explicit as well as implicit models can be distinguished. The former yield much more

accurate predictions of the B-term band broadening than the latter. Implicit expressions such as the Landauer–Davis expression lack the microscopic information about the bed geometry, and therefore only hold over a narrow range of retention coefficients, especially when assuming that the coordination number z equals 6. The Landauer–Davis expression completely fails when approaching the non-porous particle packing case (i.e., for k' and k'' close to zero). The lack of a method suggesting good *a priori* values for z furthermore makes the Landauer–Davis model inappropriate for use in the field of chromatography.

Subsequently considering the class of explicit models, a wide variety of models with varying degrees of accuracy exist. For perfectly ordered sphere packings, expression are available that are even accurate up to 9th order in ε_e. Very fortunately, liquid chromatography is performed under conditions where the permeability of the particles is of the same order of magnitude as the permeability of the surrounding medium (mobile phase filling up the interstitial void). Hence, the effective diffusivity and permeability is only weakly sensitive to the exact arrangement of the particle and void zone. This also explains why the most simple of all explicit EMT-models (i.e., the Maxwell-based model) constitutes a very good approximation (only a few % deviation from the highest accuracy solutions) over most part of the usual retention range, despite the dilute suspension assumption it is based on. An exception occurs for very small k' (approaching the impermeable particle limit) and very large values of k', where higher order expressions such as the Cheng–Torquato expression should be used.

The difference between the Maxwell-model and the highly accurate random packing model is everywhere less than 4%. Depending on the intra-particle diffusion rate, the Maxwell-model is even accurate to within 1% in the range of $0.1 < k' < 5.2$ for the case of $D_{part}/D_m = 0.5$ and in the range of $1.6 < k' < 30$ for the case of $D_{part}/D_m = 0.1$.

Using the fully exact Hashin–Shtrikman theory for coated spheres and cylinders, the explicit EMT-expressions can be extended to include the effect of the presence of a solid core, as encountered in porous-shell particles. According to this theory, the individual porous-shell particles can still be represented as a uniform zone, despite the presence of a large solid core. The effect of the latter can namely simply be expressed using an intra-particle obstruction factor γ_{part}, given by $\gamma_{part} = 2/(2+\rho^3)$ for spherical particles and $\gamma_{part} = 1/(1+\rho^3)$ for cylinders.

The same Hashin–Shtrikman theory can also be used to establish an alternative expression for the diffusion coefficient in the meso-porous zone D_{pz}. Traditionally, it is assumed that the diffusion in the meso-pores (unretained state) and in the stationary phase (retained state) occurs in parallel. This leads to a residence time weighted (RTW) expression wherein each independent diffusion process has its own obstruction factor. Using the Hashin–Shtrikman theory, an alternative expression for D_{pz} can be established that displays a very similar dependency on k' as the RTW-model, but does not rely on the use of some (*a priori* unknown) obstruction factors. It is furthermore also guaranteed to obey the physical diffusion bounds of the EMT.

The Maxwell- and the Torquato-based EMT-expressions can also be reformulated (see Section 5) into an analytical expression that can be used to derive the value of the intra-particle diffusion coefficient (D_{part}) from a peak parking measurement of γ_{eff} or from an experimental value of the B-term constant. Using these expressions, it could be demonstrated that the traditionally employed RTW-model yields D_{part}-values that display an erroneous retention factor dependency (false apparent monotonous decrease of D_{part} with increased retention), even in cases where the RTW-model appears to be able to produce a close fit to the peak parking measurements (see e.g., the $D_{part}/D_m = 0.1$-case in Fig. 4b).

Symbols

a_1, a_2	coefficients in Eq. (19b), values see Table 1
A	see Eq. (21b)
b_1, b_2, b_3, ...	coefficients in Eq. (18b), values see Table 1
B	B-term constant, see Eq. (4)
$C_{m,eq}$	equilibrium concentration of analytes in the mobile phase [mol/m^3]
d	diameter [m]
D	diffusion coefficient [m^2/s]
D_1	diffusion coefficient in zone 1 [m^2/s]
D_{eff}	effective diffusion coefficient [m^2/s]
$D_{eff,Maxwell}$	effective diffusion coefficient calculated with Maxwell expression [m^2/s]
D_m	molecular diffusion coefficient [m^2/s]
D_{part}	intra-particle diffusion coefficient [m^2/s]
D_{pz}	diffusion coefficient in porous zone [m^2/s]
D_s	diffusion coefficient in the stationary phase [m^2/s]
$F(\lambda)$	hindrance factor
h_B	dimensionless B-term plate height contribution ($=H_B/d_{part}$)
H_B	B-term plate height contribution [m]
k'	phase retention factor
k''	zone retention factor
k''_0	zone retention factor of an unretained component
K	equilibrium distribution constant, see Eq. (8)
$m_{part,eq}$	mass of analyte present in a particle at equilibrium [mol]
n	dimension, see Eq. (40c)
P	permeability [m^2/s]
$\langle P \rangle$	see Eq. (40b) [m^2/s]
$\langle \overline{P} \rangle$	see Eq. (40b) [m^2/s]
S	solubility
t_0	residence time of an unretained marker [s]
u_0	velocity of an unretained component [m/s]
V	volume [m^3]
z	coordination number as occurring in Landauer–Davis models

Greek symbols

α	permeability ratio, see Eq. (11)
β_1, β_2, β_3, ...	see Eq. (18c)
δ	Hashin-fitting factor in Eq. (20)
δ_s	thickness of the stationary phase layer [m]
ε_{cp}	porosity at the close packing limit
ε_e	external porosity
ε_{part}	particle based porosity, see Eq. (38)
ε_{pz}	porosity of the porous zone
ε_T	total porosity ($\varepsilon_T = \varepsilon_e + (1-\varepsilon_e)\varepsilon_{part}$)
ϕ	volumetric fraction
γ_e	obstruction factor in the RTW-model
γ_{eff}	effective obstruction factor
γ_{mp}	meso-pore obstruction factor
γ_{np}	obstruction factor of a packing packed with non-porous particles
γ_{part}	intra-particle obstruction factor
$\gamma_{eff,RTW}$	effective obstruction factor according to the RTW-model
γ_s	stationary phase obstruction factor
λ	ratio of the molecular diameter to the meso-pore diameter
Λ	see Eq. (18b)
ν_0	reduced velocity of an unretained component ($=u_0 d_{part}/D_m$)
ρ	relative core diameter ($\rho = d_{core}/d_{part}$)
σ	conductivity (ex. thermal) [W/m K]
τ	intra-particle tortuosity

ξ_2 Torquato's three-point factor

Subscripts

1	phase 1
2	phase 2
A,pz	relating to analyte A in porous zone
crit	critical conditions wherein permeability and diffusivity in particle and mobile zone are identical
core	core
eff	effective
i	interstitial zone (=mobile zone)
m	mobile zone
part	particle-based
pz	porous zone-based
s	stationary phase
sol	solid zone

Appendix A. Supplementary data

Supplementary data associated with this article can be found, in the online version, at doi:10.1016/j.chroma.2010.10.087.

References

[1] J.H. Knox, H.P. Scott, J. Chromatogr. 282 (1983) 297.
[2] R.W. Stout, J.J. Destefano, L.R. Snyder, J. Chromatogr. 282 (1983) 263.
[3] J.C. Giddings, Dynamics of Chromatography. Part 1, Marcel Dekker, New York, 1965.
[4] G. Desmet, K. Broeckhoven, J. De Smet, S. Deridder, G.V. Baron, P. Gzil, J. Chromatogr. A 1188 (2008) 171.
[5] K. Broeckhoven, D. Cabooter, F. Lynen, P. Sandra, G. Desmet, J. Chromatogr. A 1188 (2008) 189.
[6] S. Torquato, Random Heterogeneous Materials, Springer Science & Business Media, New York, 2002.
[7] H.T. Davis, J. Am. Ceram. Soc. 60 (1977) 499.
[8] E.L. Cussler, Diffusion Mass Transfer in Fluid Systems, Cambridge University Press, Cambridge, UK, 1984.
[9] M. Barrande, R. Bouchet, R. Denoyel, Anal. Chem. 79 (2007) 9115.
[10] F. Gritti, I. Leonardis, J. Abia, G. Guiochon, J. Chromatogr. A 1217 (2010) 3819.
[11] F. Gritti, G. Guiochon, AIChE J., doi:10.1002/aic.12280.
[12] C. Maxwell, Treatise on Electricity and Magnetism, vol. 1, Oxford University Press, London, 1873.
[13] R.C. McPhedran, D.R. McKenzie, Proc. R. Soc. Lond. A 349 (1978) 45.
[14] A.S. Sangani, A. Acrivos, Proc. R. Soc. Lond. A 386 (1983) 263.
[15] S. Torquato, J. Appl. Phys. 58 (1985) 3790.
[16] H. Cheng, S. Torquato, Proc. R. Soc. Lond. A 453 (1997) 1331.
[17] J. Sax, J.M. Ottino, Polym. Eng. Sci. 23 (1983) 165.
[18] C.M. Zimmerman, A. Singh, W.J. Koros, J. Membr. Sci. 137 (1997) 145.
[19] Z. Hashin, S. Shtrikman, J. Appl. Phys. 33 (1962) 3125.
[20] B. He, N. Tait, F.E. Regnier, Anal. Chem. 70 (1998) 3790.
[21] M. De Pra, W.T. Kok, J.G.E. Gardeniers, G. Desmet, S. Eeltink, J.W. van Nieuwekasteele, P.J. Schoenmakers, Anal. Chem. 78 (2006) 6519.
[22] W. De Malsche, H. Eghbali, D. Clicq, J. Vangelooven, H. Gardeniers, G. Desmet, Anal. Chem. 79 (2007) 5915.
[23] K. Miyabe, G. Guiochon, J. Phys. Chem. B 106 (2002) 8898.
[24] F. Gritti, G. Guiochon, J. Chromatogr. A 1216 (2009) 4752.
[25] J.H. Knox, J. Chromatogr. Sci. 15 (1977) 352.
[26] D.A. Robinson, S.P. Friedman, Physica A 358 (2005) 447.
[27] L. Rayleigh, Philos. Mag. 34 (1892) 481.
[28] R.C. McPhedran, G.W. Milton, Appl. Phys. A 26 (1981) 207.
[29] C.A. Miller, S. Torquato, J. Appl. Phys. 68 (1990) 5486.
[30] D.J. Jeffrey, Proc. R. Soc. Lond. A 335 (1973) 355.
[31] Z. Hashin, J. Comp. Mater. 2 (1968) 284.
[32] R. Landauer, J. Appl. Phys. 23 (1952) 779.
[33] D.A.G. Bruggeman, Ann. Phys. 416 (1935) 636.
[34] J. Crank, The Mathematics of Diffusion, 2nd ed., Clarendon Press, Oxford, 1975.
[35] F. Gritti, G. Guiochon, Chem. Eng. Sci. 61 (2006) 7636.
[36] H. Kobayashi, D. Tokuda, J. Ichimaru, T. Ikegami, K. Miyabe, N. Tanaka, J. Chromatogr. A 1109 (2006) 2.
[37] K. Miyabe, Y. Matsumato, G. Guiochon, Anal. Chem. 79 (2007) 1970.
[38] F. Gritti, G. Guiochon, Anal. Chem. 78 (2006) 5329.
[39] F. Gritti, A. Cavazzini, N. Marchetti, G. Guiochon, J. Chromatogr. A 1157 (2007) 289.
[40] M. Suzuki, J.M. Smith, Chem. Eng. J. 3 (1972) 256.
[41] J. Comiti, M. Renaud, Chem. Eng. Sci. 44 (1989) 1539.
[42] N. Wackao, J.M. Smith, Chem. Eng. Sci. 17 (1962) 825.
[43] K. Miyabe, N. Ando, G. Guiochon, J. Chromatogr. A 1216 (2009) 4377.
[44] A. Cavazzini, F. Gritti, K. Kaczmarski, N. Marchetti, G. Guiochon, Anal. Chem. 79 (2007) 5972.
[45] K. Miyabe, G. Guiochon, Anal. Chem. 72 (2000) 5162.
[46] K. Miyabe, M. Ando, N. Ando, G. Guiochon, J. Chromatogr. A 1210 (2008) 60.
[47] S. Torquato, G. Stell, J. Beasley, Int. J. Eng. Sci. 23 (1985) 385.